Electrochemical Characteristics of Intermetallic Phases in Aluminum Alloys

An Experimental Survey and Discussion

N. Birbilis*,z and R. G. Buchheit*

Fontana Corrosion Center, Department of Materials Science and Engineering, The Ohio State University, Columbus, Ohio 43210, USA

This paper presents a survey of corrosion potentials, pitting potentials, and electrochemical characteristics for intermetallic particles commonly present in high-strength aluminum-based alloys. Results from relevant pure metals and solid solutions are also presented. It is seen that corrosion potentials and pitting potentials vary over a wide range for various intermetallics. Elaboration of the results reveals that the electrochemical behavior of intermetallics is more detailed than the simple noble or active classification based upon corrosion potential or estimated from the intermetallic composition. Intermetallics capable of sustaining the largest cathodic current densities are not necessarily those with the most noble E_{corr}, similarly those with the least noble E_{corr} will not necessarily sustain the largest anodic currents. The data herein was collected via the use of a microcapillary electrochemical cell facilitating electrode investigations upon intermetallic particles in the micrometer-squared range. This survey may be used as a tool for clarification of localized corrosion phenomena in Al alloys.
© 2005 The Electrochemical Society. [DOI: 10.1149/1.1869984] All rights reserved.

Background.—The desirable mechanical properties of many commercial aluminum alloys are developed as a result of heterogeneous microstructures, stimulated by careful alloying additions and heat-treatments. This is especially true in high strength Al alloys for aerospace applications.[1] From a localized corrosion perspective, the dominant feature of alloy microstructures is the distribution of second-phase (intermetallic) particles.[2] Commonly such particles will exhibit electrochemical characteristics that differ from the behavior of the matrix, rendering the alloy susceptible to localized forms of corrosion. Over the years, a number of studies have been carried out in order to assess the effect of specific intermetallic particles and individual alloying additions upon corrosion accumulation in Al alloys,[3-13] which initiates from pitting-type corrosion.

Pit initiation is generally believed to begin by the rupture or breakdown of passive film upon the metal surface.[14] In the case of pure metals, pitting resistance is dependant upon the electrochemical stability of the passive film. However in the case of Al alloys, pitting is influenced by the intermetallic particles which exhibit different surface film characteristics to the matrix,[15] and may be either anodic or cathodic relative to the matrix.[8] In Al alloys, two main types of pit morphologies are observed.[16-18] So called circumferential pits appear as a ring of attack around a more or less intact particle or particle colony. The attack appears to be mainly in the matrix phase. This type of morphology has been ascribed to localized galvanic attack of the more active matrix by the more noble particle. Leclère and Newman[19] offered another interpretation based on local pH gradients, consistent with the concept of cathodic corrosion.

The second morphology is apparent selective dissolution of the constituent particle. Pits of this type are often deep and may have remnants of the particle in them.[16] This morphology has been interpreted as particle fall-out, selective particle dissolution in the case of electrochemically active particles, or in the case of some Cu-bearing particles, particle dealloying and non-faradaic liberation of the Cu component.[20]

The different variety of particles that may appear in Al alloys is vast,[1,21-23] however those which may appear in 7XXX series alloys[21] are of great technical interest and predominantly dealt with in this paper. In order to understand the electrochemical behavior of such classes of alloy, a comprehensive study on the electrochemical behavior for the range of intermetallic particles which can be present, is warranted. How constituent particle-induced pitting manifests itself is a matter of some importance for emerging damage accumulation models. For these models to be predictive, it is necessary to develop a comprehensive, self-consistent accounting of this type of pitting. In cases where the electrochemical characteristics of constituent particles have been rigorously characterized, they have been found to be much richer and more complicated than simple first-order characterizations like noble or active.[14] The aim of this work is to develop a detailed characterization of the electrochemical behavior of intermetallics found in AA7075, many of which are applicable to several other alloys.

Microstructure considered.—The microstructures developed in high-strength aluminum alloys such as AA7075, are complex and incorporate a combination of equilibrium and nonequilibrium phases. Typically such alloys have a chemical composition incorporating up to ten alloying elements. Such elements primarily include Zn, Mg, and Cu, however appreciable and specific amounts of Fe, Si, Cr, Ti, Zr, and Mn are often present (both as deliberate additions and as impurities). Although presently not fully understood in terms of its precise evolution, the microstructure of AA7075 is well characterized,[1,21] along with the corresponding physical metallurgy.[23] The literature quotes evidence supporting the presence of the following intermetallics in 7XXX series alloys (not all are simultaneously present, and temper and precise composition will regulate the types and proportion); Mg_2Si, $MgZn_2$, $Al_{20}Cu_2Mn_3$, $Al_{12}Mn_3Si$, Al_7Cu_2Fe, Al_2Cu, Al_2CuMg, Al_3Fe, $Al_{12}Mg_2Cr$, $Al_{20}Cu_2Mn_3$, Al_6Mn, Al_3Ti, Al_6Zr, Mg_2Al_3, $Al_{32}Zn_{49}$, and $Mg(AlCu)$.[1,22,24-27] The role of these intermetallics with respect to mechanical properties is beyond the scope of this paper; however intermetallic particles in aluminum alloys can be classified into three main types.[1]

Precipitates form by nucleation and growth from a supersaturated solid solution during natural or low-temperature artificial aging. They range in size from Angstroms to fractions of a micrometer. They can be spherical, needles, laths, plates, among other shapes.[23] When they are homogeneously dispersed, their effect on localized corrosion behavior is difficult to discern. However, when they are concentrated on grain boundaries, they may affect intergranular corrosion and stress corrosion cracking susceptibility.[11] Important alloying elements leading to precipitation in Al alloys include Cu, Mg, Si, Zn, Li.[1] Typical examples include, $MgZn_2$, Mg_2Al_3, Al_2Cu, and $Al_{32}Zn_{49}$.

Constituent particles are comparatively large and irregularly shaped. Characteristic particle dimensions range from a few tenths of a micrometer up to 10 micrometers. These particles can be

* Electrochemical Society Active Member.
z E-mail: birbilis.1@osu.edu

formed during alloy solidification and are not appreciably dissolved during subsequent thermomechanical processing. Rolling and extrusion tends to break up and align constituent particles into bands within the alloy. Often constituents are found in colonies made up of several intermetallic crystals or several different compound types. Because these particles are rich in alloying elements, their electrochemical behavior is often significantly different than the surrounding matrix phase.[2] In high strength Al alloys pitting is nominally associated with some fraction of the constituent particles present in the alloy.[16-18] A range of alloying elements are found in constituents, but Cu, Fe, Si, Mn, Mg are found most commonly.[1] Typical examples include Al_3Fe and Al_7Cu_2Fe.

Dispersoids are small particles comprising alloying elements that are highly insoluble in aluminum. Particle sizes typically range from 0.05 to 0.5 μm. Cr, Ti, Zr, and Mn are common dispersoid formers. With the possible exception of Mn the alloying elements concentrated in dispersoids are quite passive in environments where Al alloys are regularly used. These particles form at high temperatures and are present to control grain size and recrystallization behavior, hence are homogeneously dispersed. Typical examples include Al_3Ti, Al_6Mn, $Al_{20}Cu_2Mn_3$, and Al_3Zr.

In regards to localized corrosion, the intermetallics of particular interest are those which appear in the greatest proportion, either by size or by frequency. For AA7X75 such particles have been identified (in random order) as Mg_2Si, $MgZn_2$, Al_7Cu_2Fe, Al_2CuMg, Al_2Cu, and Al_3Fe[25,27-29] (however again this can vary depending upon individual temper[24]). The matrix phase of AA7X75 is nominally comprised of Al-(3-4 wt %)Zn-(2-3 wt %) Mg-(0.5-1 wt %)Cu.

Electrochemical testing of intermetallic compounds.—Electrochemical testing of intermetallic compounds synthesized in bulk form has previously been used to study localized corrosion phenomena,[3,4,6,7,10,11,30-35] namely the role of microgalvanic interactions in corrosion of Al-alloys.[32] This approach has led to developments in the understanding of corrosion accumulation, for example, it has been noted that the intermetallics Al_2Cu and Al_7Cu_2Fe are less prone to attack than Al_2CuMg (S-phase).[32] Alternatively, Liao and Wei[36] carried out studies using a zero resistance ammeter to galvanically couple Al to two separate model alloys (an Al-Fe alloy and an Al-Fe-Cu-Mn alloy). They found significant galvanic currents between Al and the model alloys, leading them to suggest galvanic coupling can lead to significant corrosion for the couples investigated. Scully and co-workers have also investigated the effect of chromate upon several Cu-bearing intermetallics,[12] whereas Newman and co-workers have studied the effect of alloying elements in Al solid solutions.[3,19]

In general, however, technical feasibilities mainly associated with the small size of intermetallic particles, and the ability to perform electrochemical characterization on the microscale have not yet allowed for several of the commonly observed intermetallics to be studied. Furthermore, the polarization behavior which contains more detailed electrochemical information as opposed to the corrosion potential alone, has not yet been characterized for a significant number of the commonly occurring intermetallics in Al alloys.

The last few years have seen significant activity in the study of microstructure-corrosion relationships for high strength Al alloys (namely AA2024 and AA7075).[16,24,37-41] These studies have involved the study of bulk alloy samples, with the techniques used to assess corrosion capable of probing information on the micro- and nanoscales. For example, Frankel and co-workers,[37] and Andreatta *et al.*[38,39] have used scanning Kelvin probe force microscopy experiments to assess local differences in the Volta potential of the alloy surface at various stages of the corrosion cycle. Information regarding corrosion damage morphology has also been gathered by use of fluorescence microscopy[16] and confocal scanning laser microscopy.[40] The abovementioned studies have added immensely to the understanding of the extent and morphology of damage accumulation upon such alloys, but have not provided fundamental in-

formation regarding the electrochemical characteristics of intermetallic particles. Andreatta and co-workers[42] have recently employed the use of an electrochemical microcell (which they denote as a microcapillary cell) for obtaining localized polarization data upon AA7075. Although this technique may significantly reduce the area of the working electrode, the reductions are not significant enough to isolate individual particles or even particle-matrix interfaces. Consequently, the results reflect testing upon a heterogeneous electrode surface and again do not provide specific information regarding intermetallic electrochemistry.

One major limitation of most of the studies discussed above, is that the discussion of intermetallic particles is, often necessarily, based upon qualitative assessments of intermetallic identification. Although most often analyzed by energy dispersive X-ray spectroscopy (EDXS), the EDXS method is not entirely accurate (independently) in the identification of intermetallics, since X-rays may and, most likely will, come from deeper within the sample than the intermetallic extends. This has led some authors to identify intermetallics more broadly, for example Al-Mg particles.[14,37]

Microelectrochemical testing.—In this study, we have employed the synthesis of intermetallic analogs by specific casting. Following this, electrochemical characterization was carried out via the use of a microcapillary electrochemical cell[42-46] (denoted in this work simply as microcell) capable of performing electrochemical testing on electrode surfaces in the micrometer squared range.
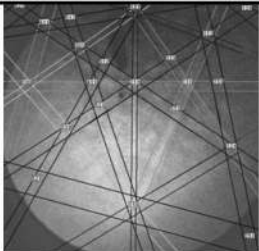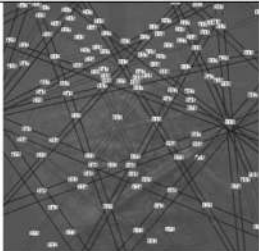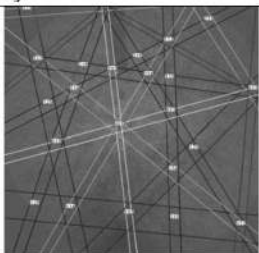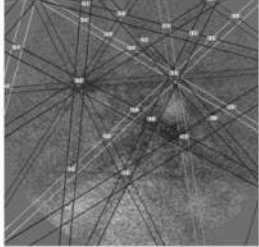
Electrochemical testing using microelectrodes has become rather widespread over the past decade,[24,32,43-46] owing to the simplicity of the methodology involved. In essence, microelectrochemical testing may be considered identical to regular (bulk) electrochemical testing, except that the size of the working electrode is reduced. This is achieved by defining a working electrode as the area of metal that comes into contact with a carefully placed solution, which either takes the form of liquid droplet head, or the solution contained with a capillary opening in the micrometer squared range.[45] The critical requirement of microelectrochemical testing is that the potentiostat being used is capable of measuring low currents (typically $< 10^{-10}$ A), since the working electrode area, hence associated current, will be very small.

Experimental

Intermetallic synthesis.—Intermetallic particles were synthesized by combining the necessary proportions of constituent pure metals (supplied by Alfa-Aeser). Satisfactory synthesis of such particles requires prior knowledge of equilibrium conditions under which the intermetallic in question will form. As a result, an equilibrium phase diagram including the intermetallic required was sourced and the composition required to fall within the appropriate phase field was used. In many cases, intermetallics do not appear in a unique phase field, and will appear in conjunction with other phases.[21] Consequently the feedstock proportions may not be indicative of the stoichiometry of the intermetallic, but indicative of the phase field which includes the given intermetallic. The appropriate phase diagrams for phases present in Al alloys are readily available throughout the physical metallurgy literature.[21]

Melting was carried out via two methods; either by induction melting, or by arc melting. In all cases an argon atmosphere and slight vacuum conditions were employed, as a safeguard to avoid oxidation and vaporization, in order to produce laboratory ingots in the vicinity of 150 g. Appropriate isothermal heat-treatments were then employed to stimulate growth of the desired intermetallics within the ingot or to generate the appropriate solid solution (in both cases to comply with the appropriate equilibrium phase diagram), with subsequent water quenching then carried out. In some cases, the intermetallic compounds were sourced from previous studies. The source and/or processing route for intermetallic synthesis is included in Table I. Ingots incorporating Cr-containing intermetallics, such as $Al_{12}Mg_2Cr$, could not be synthesized such that intermetallic particles would be large enough for microcell testing (hence

Table I. Physical information related to intermetallic particles used in this work.

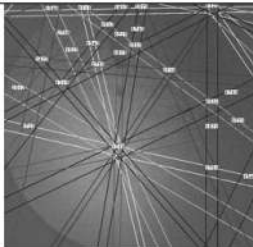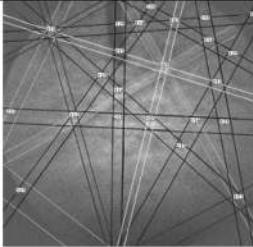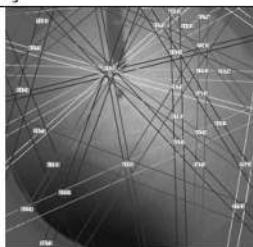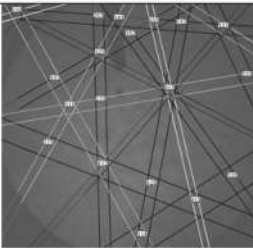| Stoichiometry	Phase	Production route	EDXS Analyses (values given to nearest atom %)	BEKP
Al_3Fe	β	Vacuum arc melting	73 Al, 27 Fe	
Al_2Cu	θ	*Sourced from [7]*		
Al_3Zr	β	*Sourced from [7]*		
Al_6Mn	-	Vacuum arc melting	82 Al, 38 Mn	
Al_3Ti	β	*Sourced from [34]*		
$Al_{32}Zn_{49}$	T'	Induction furnace	42 Al, 58 Zn	
Mg_2Al_3	β	Induction furnace	62 Al, 38 Mg	

they are not discussed any further). A requirement of subsequent-electrochemical testing via the microcell method dictated by capillary tip diameter within our laboratory, was that intermetallic particles were larger than 50 μm in each of their surface dimensions. Consequently, provided a small number of such particles were produced, then replicated electrochemical testing could be done.

It should be emphasized that the synthesis of homogeneous bulk (multigrained) intermetallic ingots is not readily possible. This is owing to the fact that most intermetallics will not develop into single-phase ingots under equilibrium conditions. Consequently, it is not our methodology to create bulk (defect-free) single-phase intermetallic ingots. Instead, we are aiming to develop an ingot that will include a population of the intermetallic crystals in question, in a size range suitable for microcell testing. This therefore takes the emphasis away from ingot production, and transfers it towards intermetallic characterization within the ingot. We do not advocate the general use of bulk intermetallic analogs since it is difficult to ensure that the ingot is indeed homogeneous and indicative of the intermetallic (furthermore bulk ingots will include grain boundaries which may differ significantly in composition with respect to the bulk ingot).

In order to evaluate the electrochemical behavior of the matrix phase of AA7075, it was decided to use a particle-free matrix equivalent. As a result, the matrix phase of AA7475 was deemed to serve as an appropriate equivalent, owing to the fact that the alloys have similar amounts of Zn, Mg, and Cu (hence forming a similar solid solution), however AA7475 has very low alloy values for Fe, Si, Zr, Ti, and Mn,[1] largely avoiding the formation of inclusions, dispersoids, and submicrometer-sized particles, will largely be avoided. Another factor is the lack of particles which may act as grain nucleators or grain refiners, resulting in a slightly larger grain size than that of AA7075, hence allowing the matrix phase of AA7475 to serve as a suitable particle-free and large-phase which may be used to tentatively represent the electrochemical behavior of particle free AA7075.

Table I.   (*Continued.*)

MgZn$_2$	M, η	Induction furnace	67 Zn, 33 Mg	
Mg$_2$Si	β	Vacuum arc melting	62 Mg, 38 Si	
Al$_7$Cu$_2$Fe	-	*Sourced from [34]*		
Mg(AlCu)	-	Induction furnace	32 Mg, 33 Al, 35 Cu	
Al$_2$CuMg	S	*Sourced from [20]*		
Al$_{20}$Cu$_2$Mn$_3$	-	*Sourced from [34]*		
Al$_{12}$Mn$_3$Si	-	Vacuum arc melting	76 Al, 7 Si, 17 Mn	
Al-2%Cu	α	Induction furnace	2 Cu − Al	n/a
Al-4%Cu	α	Induction furnace	4 Cu − Al	n/a

Intermetallic identification.—Satisfactory identification of inter-metallics requires both chemical and structural information. Characterization of the intermetallics was done via a scanning electron microscopy (SEM, Philips XL-30 FEG-ESEM) enabled with quantitative energy dispersive X-ray spectroscopy (EDXS), and the facility to generate backscattered electron Kikuchi patterns (BEKPs). The EDXS was capable of providing details of the composition of the crystals being probed (Table I). In order to translate this into accurate intermetallic identification, the supplementary use of BEKPs was employed, as previously done in Ref. 20. Following application of an intense electron beam (supplied by a field emission gun), spatial resolution of intercepted backscattered electrons yielding structural information is facilitated by a carefully placed camera detector. This detector is different from that responsible for back-scattered electron imaging. Nominally the sample is tilted in the

SEM chamber (commonly to 70°) such that the sample surface is perpendicular to the detector responsible for generation of Kikuchi patterns.

A typical example of a BEKP for Al$_6$Mn is included in Fig. 1 along with the corresponding EDXS spectrum. Each intermetallic synthesized in this work has a unique crystal structure as previously determined.[21] Table I shows the simulated pattern overlays on the collected BEKPs for all synthesized samples, indicating agreement between the collected and simulated patterns. The BEKP collection and analysis was facilitated by OIM software (TSL®). Sample preparation for the generation of satisfactory BEKPs requires that the sample surface be meticulously flat (*i.e.*, polished to below 0.1 μm finish). In this work samples were prepared by metallographic polishing down to $\frac{1}{4}$ μm finish, and subsequently vibratory polished using a 0.05 μm gamma alumina suspension. This suspen-
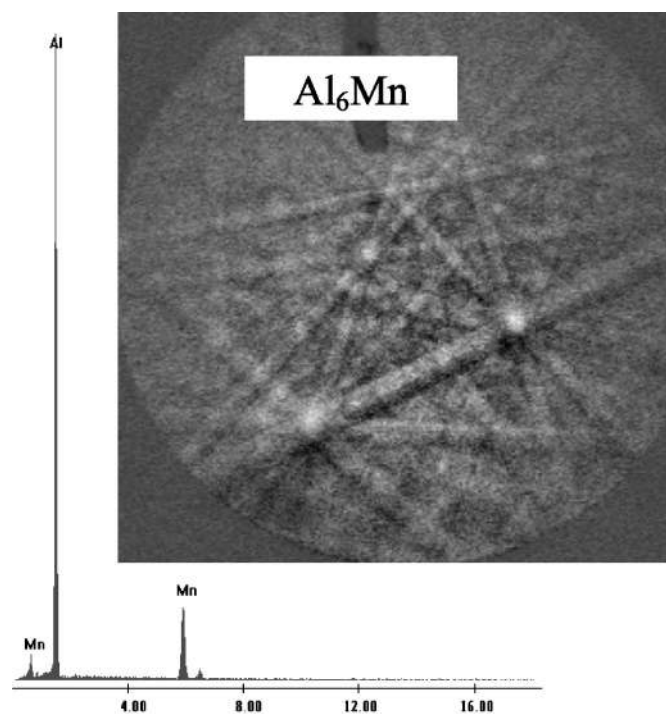
Figure 1. Backscattered electron Kikuchi pattern and corresponding EDXS spectrum for Al_6Mn crystal.

sion was chosen owing its inertness, in an effort to avoid surface dissolution.

Electrochemical characterization.—Electrochemical testing of the synthesized intermetallics was carried out using a microcell method, as outlined previously in Ref. 32 and 43-45. In this method, the working electrode area is defined by the area of metal which comes into contact with the opening of a microcapillary. The microcapillary is filled with electrolyte/solution, while containing a small wire counter electrode and electrolytic contact with a saturated calomel reference electrode. A silicone skirt/seal was applied to the open end of the capillary in order to avoid any solution leakage and to allow an interference contact with the working electrode. The capillary opening is generally in the vicinity of 20-60 μm diam, and will vary with each capillary. Therefore, each test must be treated individually to establish the correct working electrode area for determination of current *density* values. A series of schematics and pictures is included as Fig. 2, showing various aspects of the microcell method as adopted in this work. Figure 2a indicates a schematic of the electrochemical cell component used to carry out testing. A more complete set of pictures covering apparatus and setup can be found in Ref. 44. Figure 2b indicates a typical microcapillary used, with the silicone skirt clearly visible. As an example to the spatial resolution of the method, a picture of an $Al_{20}Cu_2Mn_2$ crystal is shown prior to electrochemical testing and also following testing (Fig. 2c and d). The microcell used in these studies was incorporated into a lenspiece of an optical microscope. This made it possible to switch between viewing/aligning the sample on the microscale, and subsequent testing with the microcell. The microscope was also connected to a video output, allowing microimages to be captured digitally.

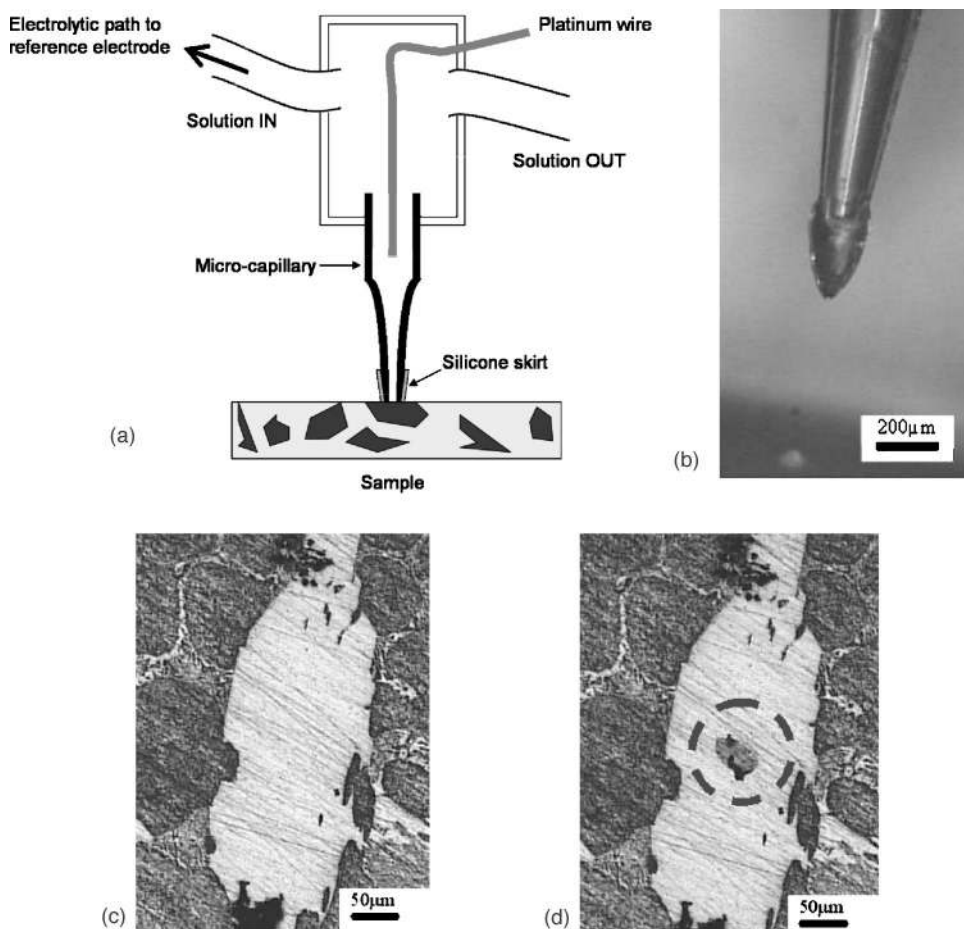Potentiodynamic polarization was carried out at a scan rate of

Figure 2. (a) Schematic representation of microcapillary electrochemical cell. (b) Glass capillary with tip coated in silicone. (c) Optical micrograph of $Al_{20}Cu_2Mn_3$ crystal prior to testing. (d) Optical micrograph of $Al_{20}Cu_2Mn_3$ crystal following electrochemical testing with the microcell. Test area is evident.

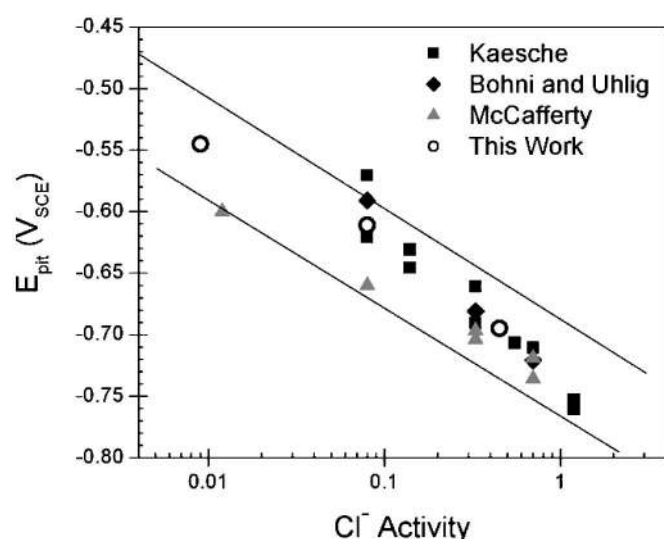**Figure 3.** Pitting potentials for aluminum presented as a function of chloride ion activity.

Figure 4. Typical polarization curves for aluminum collected using the microcell method at three different chloride concentrations at neutral pH. The values for E_{corr} and E_{pit} are noted.

0.01 V s^{-1} using an Autolab PGSTAT 100 with resolution at low currents (down to 1×10^{-15} A). Equilibration time for the working electrode was 60 s following contact with the solution. Such precautions were taken to minimize test durations, in order to avoid any issues with cell leakage, or the establishment of concentration gradients in the capillary. It should be pointed out that the nominal cell resistance (responsible for iR-drop) was comparatively high with respect to other systems, with values approaching 10 $k\Omega$ recorded. However, since the absolute currents measured during testing rarely approached values up to 10^{-7} A (owing to the small size of the working electrode), ohmic drop was considered negligible for potentiodynamic testing, since it would be nominally confined to under 1 mV. The tests reported herein should also be considered to have been carried out in aerated conditions, since no special effort was made to exclude oxygen from the capillary or solution. Each test was repeated at least six times and the average values are reported herein. Measurements were performed in 0.01, 0.1, and 0.6 M NaCl at pH 6.

Results

Verification of microcell data.—Given the relatively unique nature of electrochemical testing via the microcell method, owing to the rapid scan rates used and the short equilibration times prior to polarization, a set of control tests was initially conducted upon pure Al (99.9999). This was done in order to correlate with previously reported literature values and to verify the sensitivity of the method to variations in electrochemical response with respect to electrolyte aggressiveness. The results of breakdown/pitting potential (E_{pit}) *vs.* chloride activity are given in Fig. 3, and compared with those of McCafferty,[47] Kaesche, Bohni, and Uhlig (given in Ref. 48) who performed tests upon AA 1199 (Al 99.99). Typical potentiodynamic polarization curves that went into the construction of Fig. 3 are included in Fig. 4. The raw data in Fig. 4 was collected using the microcell method. Based upon the sensitivity of the microcell method as evidenced by the control testing upon aluminum (Fig. 3 and 4), it is posited the method is able to delineate between the electrochemical behaviors of various intermetallic particles, in spite of the relatively unique experimental parameters employed by the technique. As a result, meaningful potentiodynamic diagrams may be obtained.

Electrochemical behavior of intermetallic particles.—The corrosion potentials (E_{corr}) for the compounds tested in this study are given in Table II. Table II also includes information relating to rel-
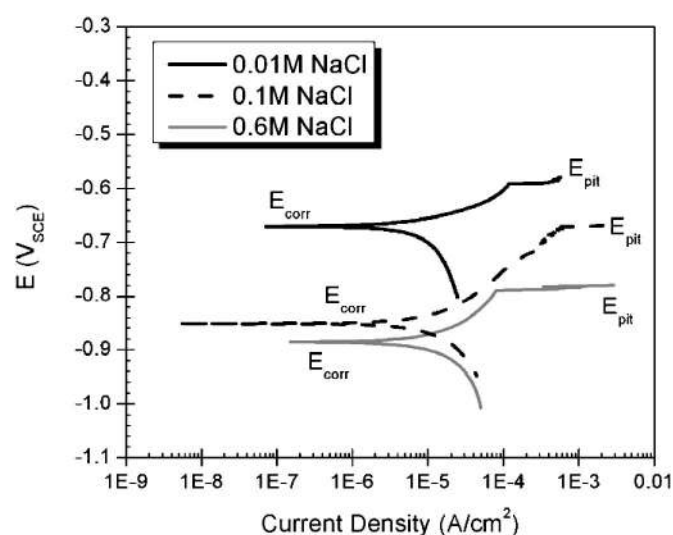
evant pure metals, solid solutions, and an analog to the matrix phase of AA7075.

Table II. Corrosion potentials for intermetallic compounds common in aluminum alloys. Results are average values incorporating the results of numerous tests.

Stoichiometry	Phase	Corrosion potential (mV$_{SCE}$)			Note
		0.01 M	0.1 M	0.6 M	
Al$_3$Fe	β	−493	−539	−566	
Al$_2$Cu	θ	−592	−665	−695	
Al$_3$Zr	β	−752	−776	−801	
Al$_6$Mn	-	−839	−779	−913	
Al$_3$Ti	β	−620	−603	−799	
Al$_{32}$Zn$_{49}$	T′	−1009	−1004	−1063	
Mg$_2$Al$_3$	β	−1124	−1013	−1162	
MgZn$_2$	M, η	−1001	−1029	−1095	
Mg$_2$Si	β	−1355	−1538	−1536	
Al$_7$Cu$_2$Fe	-	−549	−551	−654	
Mg(AlCu)	-	−898	−943	−936	
Al$_2$CuMg	S	−956	−883	−1061	
Al$_{20}$Cu$_2$Mn$_3$	-	−550	−565	−617	
Al$_{12}$Mn$_3$Si	-	−890	−810	−858	
Al (99.9999)	-	−679	−823	−849	A
Cu (99.9)	-	−177	−232	−220	A
Si (99.9995)	α	−450	−441	−452	A
Mg (99.9)	-	−1601	−1586	−1688	A
Mn (99.9)	-	−1315	−1323	−1318	A
Cr (99.0)	-	−495	−506	−571	A
Zn (99.99)	-	−985	−1000	−1028	A
Al-2%Cu	α	−813	−672	−744	B
Al-4%Cu	α	−750	−602	−642	B
7X75 Matrix	-	−699	−799	−812	M
AA 7075-T651	-	−816	−965	−1180	X

Notes:
A. Pure metal were obtained from Alfa-Aeser and tested using the microcell method.
B. These specimens are homogeneous solid solutions and tested using the microcell method.
M. The phase denoted as 7X75 matrix is the particle-free matrix-phase of AA7474.
X. Tests upon AA7075-T651 were done on bulk specimens using conventional electrochemical methods and an electrode area of 1 cm^2.

Table III. Pitting potentials for intermetallic compounds common in aluminum alloys. Results are average values incorporating the results of numerous tests.

| Stoichiometry | Phase | Pitting potential (mV_{SCE}) | | | Note |
		0.01 M	0.1 M	0.6 M	
Al_3Fe	β	442	106	−382	
Al_2Cu	θ	−434	−544	−652	
Al_3Zr	β	−223	−275	−346	
Al_6Mn	-	−485	−755	−778	
Al_3Ti	β	−232	−225	−646	
$Al_{32}Zn_{49}$	T′	-	-	-	C
Mg_2Al_3	β	−818	−846	−959	
$MgZn_2$	M, η	-	-	-	C
Mg_2Si	β	-	-	-	C
Al_7Cu_2Fe	-	−447	−448	−580	
Mg (AlCu)	-	224	−2	-	D, E
Al_2CuMg	S	108	80	135	F
$Al_{20}Cu_2Mn_3$	-	−210	−428	−534	
$Al_{12}Mn_3Si$	-	−563	−621	−712	
Al (99.9999)	-	−545	−610	−696	A
Cu (99.9)	-	19	−30	−94	A
Si (99.9995)	α	-	-	-	A, C
Mg (99.9)	-	−1095	−1391	−1473	A, G
Mn (99.9)	-	-	-	-	A, C
Cr (99.0)	-	479	297	190	A
Zn (99.99)	-	-	-	-	A, C
Al-2%Cu	α	−447	−471	−529	B
Al-4%Cu	α	−418	−406	−465	B
7X75 Matrix	-	−633	−736	−768	M
AA 7075-T651	-	−684	−739	−810	X

Notes:

C. These compounds do not shows a breakdown of passivity, with active dissolution occurring at potentials more positive than E_{corr}.

D. Did not show a breakdown in all cases when tested at 0.1 M NaCl.

E. At the highest concentration of NaCl tested, this compound did not display a breakdown of passivity, with active dissolution occurring at potentials more positive than E_{corr}.

F. The breakdown potential (E_{pit}) of S-phase should be viewed with caution. The electrochemical behavior of this compound is complex[20] and incorporates dealloying of the Al and Mg, capable of generating a relatively large corrosion current density prior to ultimate breakdown. For more details regarding S-phase, see Ref. 20 and 30.

G. The quoted E_{pit} values of pure Mg correspond with the potential at which current density rapidly increases. Pure Mg, however, is generally unstable and freely corrodes in Cl-containing solution.

The corresponding pitting potentials (E_{pit}) for the compounds tested in this study are given in Table III. We note that not all compounds tested show a characteristic breakdown potential. In such cases, corrosion current gradually increases as potentials more anodic than E_{corr} are realized. Such compounds do not show any passivity and hence corrode freely above E_{corr}.

The data provided in Tables II and III incorporates the results of an extensive test program. As previously suggested, not all the compounds listed in Tables II and III will play a key role in determining the overall corrosion kinetics of AA7075. Those which are postulated to be of principal significance are those which were previously recognized as being present in the largest size and frequency. However, the complete list of compounds has been presented as it forms a crucial part of this experimental survey, while the intermetallics listed are relevant to a large number of commercial Al alloys.

Overall, a sense of the relative nobility for the compounds tested may be gained by examination of Tables II and III: The trends in results appear to be consistent irrespective of NaCl concentration. The net effect of increasing NaCl concentration is that both the E_{corr} and E_{pit} values are shifted to less noble values, similar to the manner seen for pure Al.[47] In some cases, this may not be entirely obvious
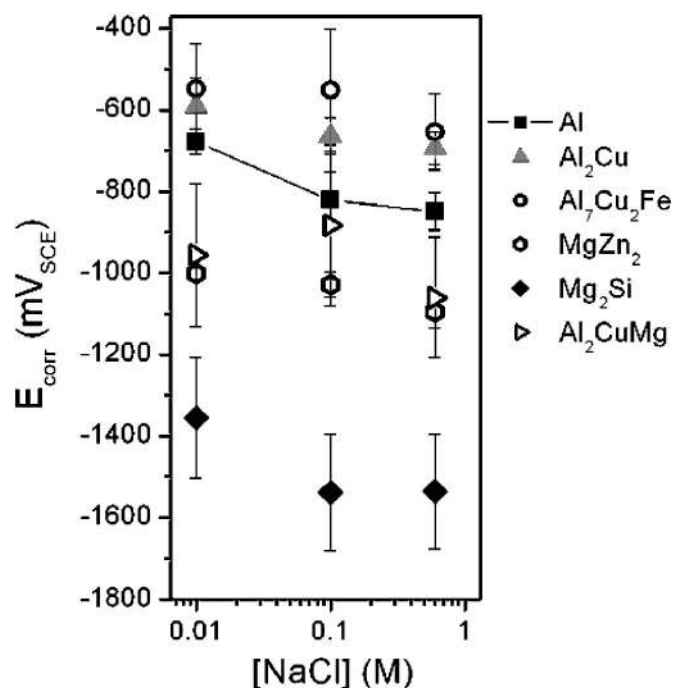
Figure 5. Corrosion potential (E_{corr}) *vs.* NaCl concentration (of test solution) for various intermetallic compounds and pure Al (99.9999).

from Table II (since the data in Table II gives the average values only). In order to visualize this, E_{corr} results for a number of intermetallics have been summarized graphically in Fig. 5, along with pure Al. Not all compounds have been plotted in order to allow a feasible number of points to be shown on one graph.

Dispersion in characteristic potentials.—From Fig. 5 it is apparent that the measured E_{corr} values vary within a range represented by the error bars between replicated tests. Typically, E_{corr} values varied within a window of about 80 mV between replicate tests, whereas E_{pit} values typically varied within about a 40 mV window. Data distribution between repeated tests is common,[34] and Figs. 6a-e show the distributions corresponding to the intermetallics Al_2Cu, Al_7Cu_2Fe, $MgZn_2$, Mg_2Si, and Al_2CuMg to serve as general examples. We note that there is dispersion in the results presented in Figs. 6a-e. However, it is unlikely that this dispersion will compromise the overall validity of the electrochemical testing herein, but merely serves to highlight that characteristic electrochemical parameters do vary within an envelope.

Results viewed with relation to corrosion of AA7075.—A montage of polarization curves generated in 0.1 M NaCl for the matrix analog and the corresponding intermetallics associated with AA7075 is presented in Fig. 7. This representation serves as a useful way in which to view a series of polarization curves. For equivalent values of potential, the individual behavior of the intermetallics *vs.* the matrix may be compared. We note that at potentials corresponding to the E_{corr} of AA7075 (in NaCl solution), $MgZn_2$ and Mg_2Si are experiencing extensive anodic dissolution. In contrast to this, at potentials corresponding to the individual E_{corr} values of Al_3Fe and Al_2Cu, the matrix is experiencing significant anodic dissolution. The interpretation of Fig. 7, along with a discussion regarding the S-phase, is expanded in the Discussion section.

Additional results for intermetallics not extensively characterized by electrochemical methods.—In order to provide additional kinetic information regarding intermetallics not previously reported in extensive detail, the typical potentiodynamic polarization curves collected in 0.1 M NaCl are shown for $Al_{32}Zn_{49}$, Mg(AlCu), Al_3Ti,
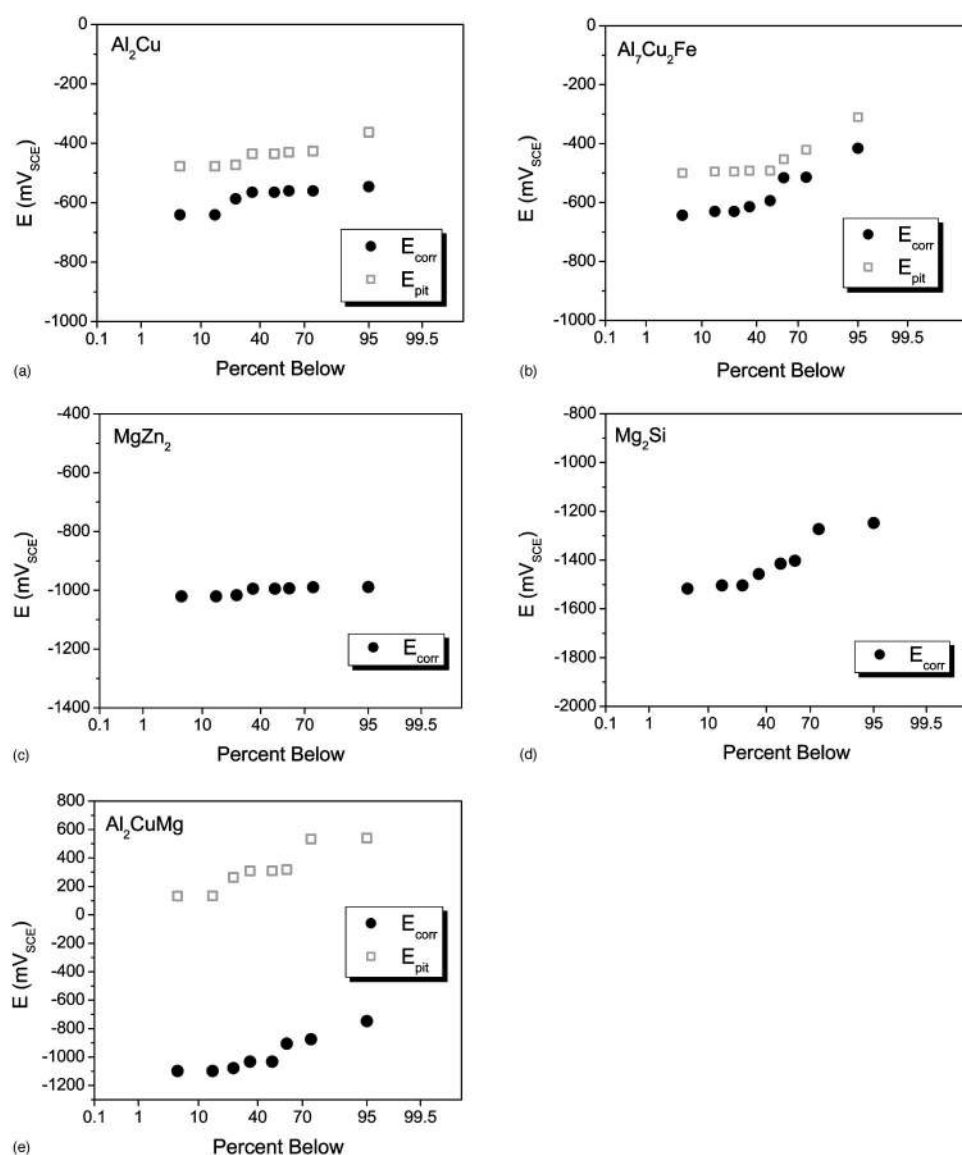
Figure 6. Distribution plots of E_{corr} and E_{pit} for (a) Al_2Cu, (b) Al_7Cu_2Fe, (c) $MgZn_2$, and (d) Mg_2Si, and (e) Al_2CuMg in 0.01 M NaCl solution.

Mg_2Al_3, $Al_{12}Mn_3Si$, and Al_7Cu_2Fe (Fig. 8a-f). These results are contrast with those already available in the literature in the following section.

Discussion

Electrochemical behavior of intermetallic particles.—The tabulated results indicate that the range of corrosion potentials observed for the different intermetallics varies over several hundreds of millivolts, reflecting the electrochemical heterogeneity that may be found in many commercial Al alloys. We note that characteristic values of E_{corr} for intermetallics are dependant upon chemical composition. It is seen that compounds containing Cu, Fe, and Ti are more noble than pure Al or the matrix analog. Such compounds include Al_3Fe, Al_7Cu_2Fe, Al_2Cu, and Al_3Ti. All of these compounds reveal a characteristic breakdown potential, indicating that they are capable of maintaining a passive film.

In contrast, intermetallics containing Mg, Zn, or Si, are typically less noble than pure Al or the matrix analog. It is noted that $Al_{32}Zn_{49}$, $MgZn_2$, and Mg_2Si do not show any breakdown potential and are capable of corroding freely above their E_{corr}. This is significant, since the latter two are present to an appreciable extent in several 7XXX series alloys.[24,25,28-30]

The reported values of the corrosion potentials determined in this study correlate with the applicable related values previously reported by other authors and compiled by Buchheit (Ref. 2 and references reported therein) or given in Ref. 11, 20, 31, 32, 34, 35, 48, and 49. As noted in this compilation, information regarding electrochemical characteristics of intermetallic compounds is not available in a unified publication; however this work has been able to draw together a large amount of characteristic data in standard test solutions to allow for a consolidated presentation. The magnitude and depth of data in Tables II and III does not permit for a complete discussion of all results in each context where they may apply, however in order to provide a working example we have focused on corrosion of AA7075 as one example.

Discussion of results viewed in relation to 7075.—In the context of AA7075, we can use the data herein to allow us to understand the evolution of corrosion damage accumulation. For example, if we recall the data presented in Fig. 7 (collected in 0.1 M), we can make certain specific assumptions regarding the corrosion morphology we expect to see. In the case of $MgZn_2$ and Mg_2Si, we would anticipate observing anodic dissolution of these intermetallic particles, ultimately leaving behind a surface cavity (selective dissolution). The reason for this is owing to the inability of these two intermetallics to passivate; hence at potentials which may be realized when polarized by/coupled to the matrix, dissolution will proceed until the interme-
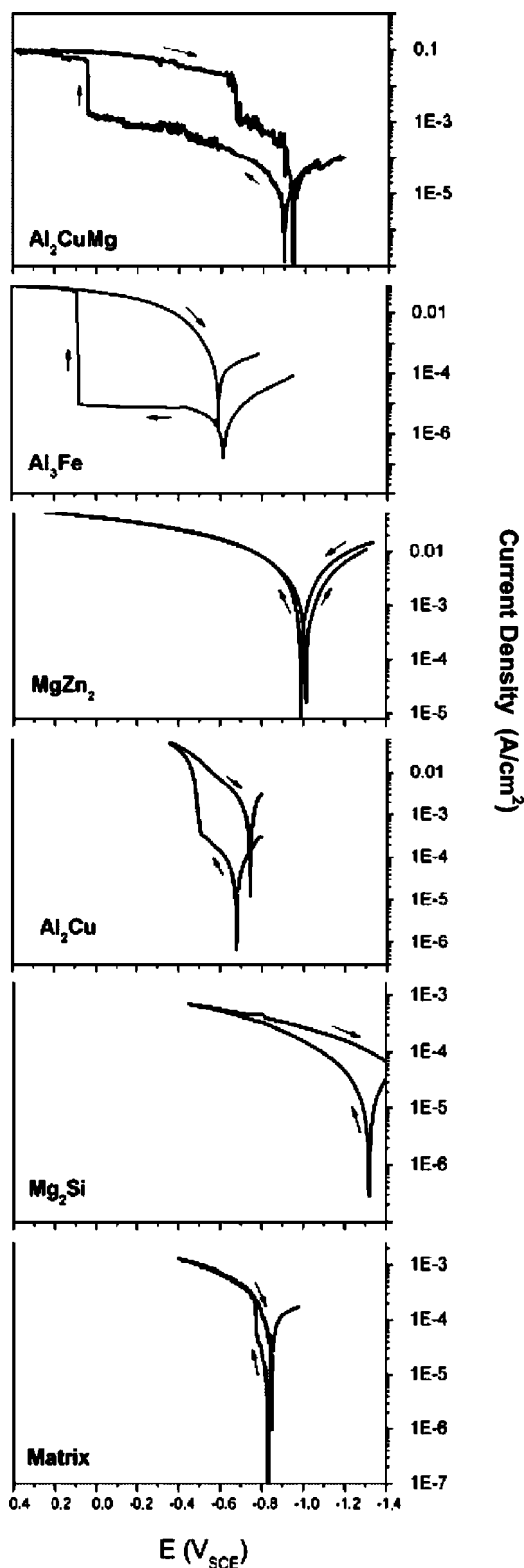
Figure 7. Montage of polarization curves for phases typically present in AA7075.

the underpinning of much of the mechanistic explanations in Al alloy corrosion science.[49] We now see an example of how little these terms account for, since the behavior of intermetallics is seen as being very rich. For example, Mg_2Si displays a value of E_{corr} several hundreds of millivolts more negative than $MgZn_2$; hence a traditional interpretation may suggest that this is the more active of the two intermetallics. Figure 7, however, reveals that across a wide range of potentials typical of the matrix, $MgZn_2$ shows anodic dissolution about two orders of magnitude greater than Mg_2Si. This phenomenon is only detectible owing to the complete electrochemical characterization of these intermetallics, and is not obvious from E_{corr} measurements and estimates based on composition alone.

In contrast, for the case of Al_2Cu and Al_3Fe, we would expect to see little or no dissolution of these noble particles. The ability of such particles to efficiently sustain cathodic reactions has been previously noted.[7] Hence, we may expect the matrix adjacent to the particle to corrode owing to the polarization provided by the noble particle and/or a localized increase in the pH (due to hydroxyl ion formation) promoting dissolution of the adjacent matrix. Evidence of so-called peripheral matrix dissolution is often observed.[16]

The richness in the behavior of intermetallic particles (IMPs) is evident again, however, in the case of Al_2Cu and Al_3Fe. Since Al_3Fe displays an E_{corr} value more noble than that of Al_2Cu (also concomitant with a more noble E_{pit}), one may expect that Al_3Fe be the most noble of the intermetallics. If this were the case, Al_3Fe should provide the largest driving force for the corrosion of the adjacent matrix. What is seen, however, is that in a wide potential range characteristic of the matrix, Al_2Cu can sustain cathodic reduction processes at rates an order of magnitude higher than Al_3Fe. Thus, traditional concepts of relative activity based upon active or noble are insufficient to describe mechanisms in overall damage accumulation.

A special note must be made regarding the electrochemical behavior of the S-phase (Al_2CuMg). The S-phase is unique since it nominally displays an E_{corr} value less noble than that of the matrix, however, the high breakdown potential may lead one to believe that the S-phase is cathodic to the matrix. The dissolution characteristics of the S phase are complex and have been shown[20] to incorporate a dealloying mechanism, leading to localized Cu enrichment. As a result, relatively large current densities prior to ultimate breakdown may be seen, with the ultimate breakdown possibly corresponding to that of nearly pure (redistributed) Cu. A detailed study regarding the electrochemical characteristics of the S-phase is not given in this paper, however more details may be found in Ref. 20 and 30. It may be assumed that the S-phase does not dissolve as a unique entity, but may undergo a dealloying process leading to selective dissolution of the Mg and Al components of the intermetallic. The result of this may be that the resultant Cu enrichment may allow for the intermetallic to behave as a local cathode after some unknown time.[37]

Elaboration of the above concepts is clearer by investigation of Table IV. Table IV lists the compounds tested in galvanic series order, based upon the evaluated E_{corr}. In the specific case of AA7075, we see that the majority of intermetallics are more noble than the matrix. Those intermetallics which are deemed less noble than the matrix are generally found to contain Mg and/or Zn.

Table IV also includes the average value of the corrosion current measured at E_{corr} during potentiodynamic testing. We nominally observe that the compounds showing the highest corrosion currents are those more active (*i.e.*, less noble) than the matrix. Such compounds are likely to be dissolving themselves at a high rate within the alloys.

Information pertaining to the average currents measured upon compounds tested at the potential corresponding to the E_{corr} of the AA7075 is also included in Table IV. This information provides a deeper insight into the overall behavior of the alloy, further indicating the weaknesses of E_{corr} values alone as a basis for mechanistic interpretations of alloy corrosion, while revealing which IMPs may warrant the most attention. It is seen that the largest currents at the

tallic is disintegrated. It may even be possible that some Mg enrichment may be observed in the presence of alkaline solutions owing to incongruent dissolution.[28]

Figure 7, however, allows us to challenge the generic concepts of noble and active as applied to intermetallics, which presently form

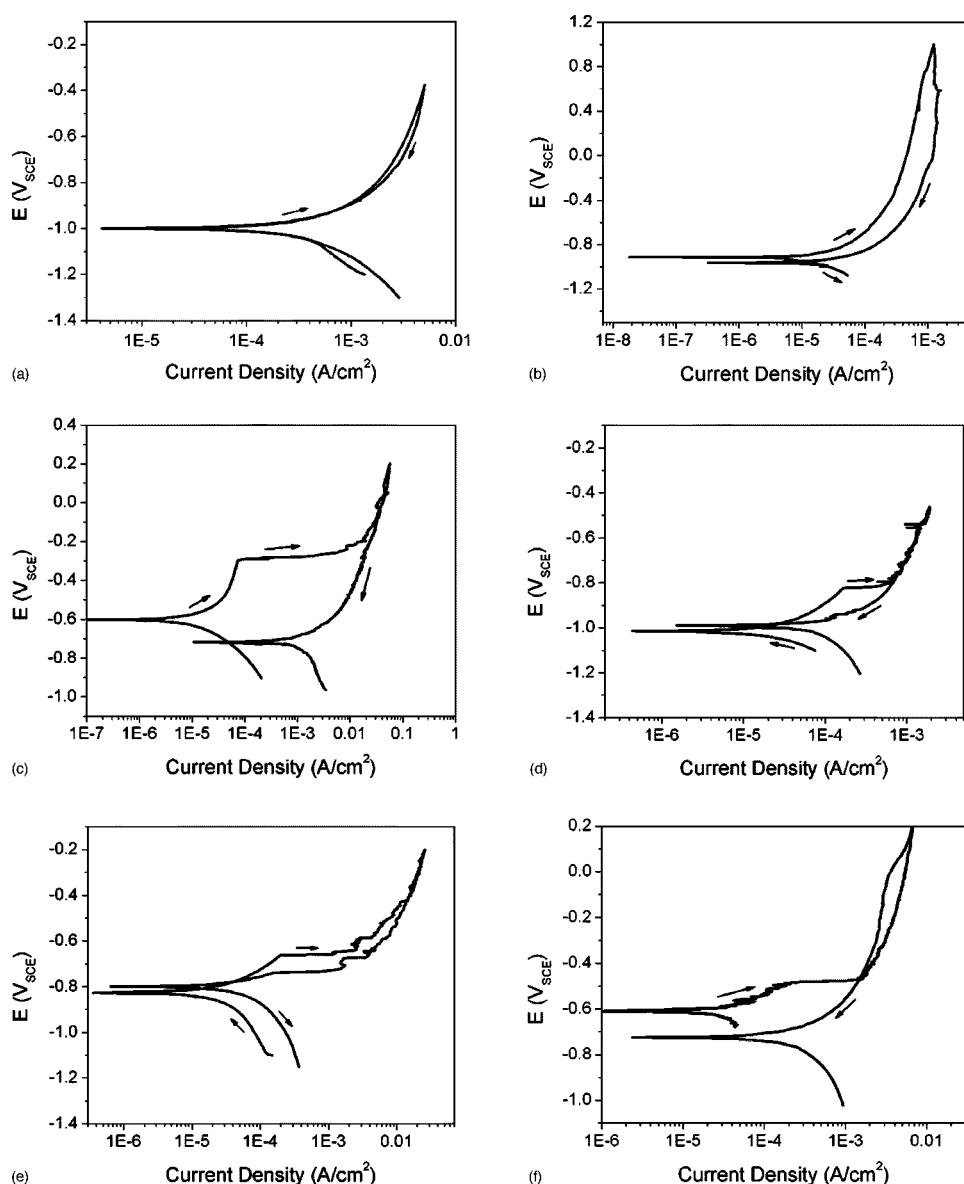**Figure 8.** Potentiodynamic polarization curves for (a) $Al_{32}Zn_{49}$, (b) Mg(AlCu), (c) Al_3Ti, (d) Mg_2Al_3, (e) $Al_{12}Mn_3Si$, (f) $Al_{17}Cu_2Fe$, generated using the microcell method and 0.1 M NaCl solution.

E_{corr} of AA7075 can be sustained by $MgZn_2$ (anodic), along with Al_7Cu_2Fe and Al_2Cu (cathodic). Hence these IMPs should form the watch list in relation to corrosion kinetics in cases where they are present. Whether these IMPs identified as the watch list are indeed primarily responsible for overall corrosion kinetics is discussed in the following section.

Electrochemical behavior of selected intermetallics not extensively characterized.—$Al_{32}Zn_{49}$.—The IMP $Al_{32}Zn_{49}$ may appear in certain 5XXX or 7XXX series alloys,[23] and has been previously discussed in the context of SCC of such alloys. It is seen that for $Al_{32}Zn_{49}$ (Fig. 8a), there is no passive region evident. At potentials more positive than E_{corr}, dissolution rates increase markedly and approach rates beyond 1 mA/cm² even for relatively modest potentials, *i.e.*, at values in the vicinity of most Al alloys.

Mg(AlCu).—Similarly, there is no evident passive region for Mg(AlCu) (Fig. 8b), however, the corresponding dissolution rates during anodic polarization remain comparatively lower than other nonpassivating compounds, even at potentials as high as +1 V_{SCE}. Mg(AlCu) can be considered analogous to $MgZn_2$ with Cu and Al substituting Zn sites. The effect of this substitution results in an

increase in the corresponding E_{corr}, and a reduction in the dissolution kinetics of the intermetallic. The presence of Mg(AlCu) has been noted in high strength 7XXX series alloys.[25]

Al_3Ti.—Al_3Ti (Fig. 8c) shows a distinct passive-active transition with E_{pit} separated from E_{corr} by about 400 mV. We also see classical positive hysteresis in the reverse scan. Al_3Ti is one of the most noble IMPs tested in this work, with an E_{corr} more positive than -0.6 V_{SCE}. The values measured here correspond well with those of Lavrenko *et al.*[31] who determined a stationary corrosion potential of -0.6 V in artificial seawater. Al_3Ti is present in several high-strength alloys, since Ti is intentionally added as an innoculant. Consequently Al_3Ti is very small and classed as a dispersoid. The effect of Al_3Ti on corrosion behavior of Al alloys has not previously received significant attention, since the submicrometer size of Al_3Ti and the ability to resolve a corrosion-IMP relationship on the nanoscale is relatively difficult.

Mg_2Al_3.—This IMP has recently received some detailed attention, since it has been associated with the SCC behavior of 5XXX series alloys. In spite of the relatively large amount of Mg present in this

Table IV. Galvanic series for compounds tested in this work.

Stoichiometry	Phase	Corrosion potential (m V_{SCE})	Average free corrosion rate at corrosion potential (A/cm^2)	Average current at corrosion potential of AA7075-T651 (A/cm^2)
Mg (99.9)	-	−1586	5.5×10^{-6}	1.5×10^{-5}
Mg$_2$Si	β	−1538	7.7×10^{-6}	1.9×10^{-4}
MgZn$_2$	M, η	−1029	8.4×10^{-5}	1.0×10^{-3}
Mg$_2$Al$_3$	β	−1013	4.8×10^{-6}	1.9×10^{-5}
Al$_{32}$Zn$_{49}$	T′	−1004	1.4×10^{-5}	2.9×10^{-4}
Zn (99.99)	-	−1000	1.2×10^{-6}	8.1×10^{-5}
AA 7075-T651	-	−965	1.07×10^{-6}	-
Mg (AlCu)	-	−943	2.3×10^{-5}	-1.2×10^{-5}
Al$_2$CuMg	S	−883	2.0×10^{-6}	-2.1×10^{-6}
Al (99.9999)	-	−823	3.9×10^{-6}	-4.7×10^{-5}
Al$_{12}$Mn$_3$Si	-	−810	1.7×10^{-6}	-7.6×10^{-5}
7X75 Matrix	-	−799	3.2×10^{-6}	-8.1×10^{-5}
Al$_6$Mn	-	−779	6.3×10^{-6}	-1.2×10^{-4}
Al$_3$Zr	β	−776	2.5×10^{-6}	-8.1×10^{-5}
Al-2%Cu	α	−672	1.3×10^{-6}	-2.1×10^{-4}
Al$_2$Cu	θ	−665	7.3×10^{-6}	-4.7×10^{-4}
Al$_3$Ti	β	−603	5.6×10^{-7}	-2.7×10^{-4}
Al-4%Cu	α	−602	2.3×10^{-6}	-2.9×10^{-4}
Al$_{20}$Cu$_2$Mn$_3$	-	−565	3.4×10^{-7}	-1.9×10^{-5}
Al$_7$Cu$_2$Fe	-	−551	6.3×10^{-6}	-3.1×10^{-4}
Al$_3$Fe	β	−539	2.1×10^{-6}	-9.9×10^{-5}
Cu (99.9)	-	−232	1.8×10^{-6}	-1.8×10^{-3}

IMP, Mg$_2$Al$_3$ shows a distinct breakdown at values just below −0.8 V_{SCE} (Fig. 8d), indicating that it has a window of passivity in the NaCl solution. This is supported by the subsequent positive hysteresis observed. It is interesting to note that breakdown occurs at a potential consistent with a relatively large current density (0.1 mA/cm^2). Furthermore the reversible potential on the reverse scan shows a slight ennoblement to that of the forward scan.

Similar testing upon synthesized Mg$_2$Al$_3$ was published by Searles and co-workers.[11] Those results were obtained in buffered solutions of aerated 3.5 pct NaCl solution, and it was seen that they correspond well with those presented here. Across a wide range of pH (3.3-13.5), Searles *et al.* quotes E_{corr} values in the vicinity of −1.25 V_{SCE}, generally about 100 mV less negative than those seen in Table II for our tests in 0.6 M NaCl. In regards to E_{pit}, consistent values in the vicinity of −0.95 V_{SCE} are seen in Ref. 11 and in Table III for tests in 0.6 M NaCl. Overall, Mg$_2$Al$_3$ may be considered active, noting that the E_{pit} value of Mg$_2$Al$_3$ are generally below the corresponding corrosion potentials for alloys in which it may be found.

Al$_{12}$Mn$_3$Si.—This IMP has previously been studied in the context of 3XXX series alloys and architectural alloys where filiform corrosion may occur.[10] Al$_{12}$Mn$_3$Si reveals a distinct breakdown, in this case at −0.6 V_{SCE} (Fig. 8e). This breakdown is associated with a slight ennoblement in the reverse scan. One possible reason for why we may observe such a slight ennoblement for the above two intermetallics may be due to selective dissolution of the more active components, viz. Mg and Si, during the anodic cycle; however this has not been independently confirmed in this work.

Although this IMP is generally classed as noble with respect to the remainder of bulk alloys, we note that in the potential range characteristic of many Al alloys, say between −0.8 to −1 V_{SCE}, that Al$_{12}$Mn$_3$Si does not show high rates of oxygen reduction. This may suggest that this IMP does not play a significant role in the overall corrosion of the alloys in which it is dispersed. This was supported in a study by Afseth *et al.*[10] where testing revealed that Al$_{12}$Mn$_3$Si did not have any discernable impact on the corrosion of AA3005.

Al$_7$Cu$_2$Fe.—The compound Al$_7$Cu$_2$Fe has recently been discussed as a contributor to localized damage accumulation upon AA2024[12] and AA7075.[40] This IMP shows a relatively noble E_{corr} value (in the vicinity of −0.6 V_{SCE}) with respect to other intermetallics listed in Table II. Concomitantly the E_{pit} value, which is very distinct, occurs at values of −0.45 V_{SCE}, followed by positive hysteresis (Fig. 8f). The effect of both Cu and Fe also allows for Al$_7$Cu$_2$Fe to sustain relatively large cathodic current densities (Table IV), indicating that it may be an archetypal noble particle with low dissolution rate and a high efficiency for supporting oxygen reduction.

General.—Although Table IV reveals that a large number of intermetallics show electrochemical activity, not all compounds listed may significantly impact corrosion kinetics. For example, as previously mentioned, due to their small size, homogenous dispersion and comparative electrochemical inertness, dispersoids do not appear to have a significant direct effect on localized corrosion susceptibility in high-strength aluminum alloys. A search of the literature does not reveal any evidence that Al$_{20}$Cu$_2$Mn$_3$, Al$_3$Zr, Al$_3$Ti, and Al$_{12}$Mn$_3$Si have impacted adversely on corrosion properties of commercial Al alloys. Consequently in the interpretation and application of the data included in this study, the effect of intermetallic size should be considered (as this will govern the amount of current the intermetallic can support). Intermetallics rich in Cu or Fe are nominally orders of magnitude larger in size than dispersoids and nominally capable of supporting oxygen reduction much more efficiently.

Although not discussed in great detail, the supplementary data included in Tables II and IV regarding (Al-Cu) solid solutions and pure metals (Al, Mg, Mn, Zn, Si, and Cu) can help describe the behavior of intermetallics and the role of pure elements in destabilizing the passive film or enhancing oxygen reduction kinetics. These results also form an important aspect of this survey for prospective users of this data.

The results presented herein for the Al-Cu solid solutions may be discussed in accordance with the results of Leclère and Newman,[19] where by the increase in Cu content allows for enhanced oxygen reduction. This, however, raises an important point regarding inter-

metallic and alloy corrosion, in that overall more corrosion has been previously observed upon samples richer in Cu. This is contradictory to the simple noble and less noble concepts, which we are challenging, and has been credited to local enrichment sites of Cu which have the ability to function as pure cathodes ultimately leading to incongruent (self) dissolution. Such incongruent dissolution has also been observed upon the S-phase,[20] and may indeed form the basis of self-corrosion for several of the intermetallics investigated in this study. Consequently, further refinements to the classifications herein based on surface analysis will allow us to account for changes in electrochemical behavior with time or as a function of environment due to the evolution of the surface film by incongruent dissolution or dealloying.

Consequently we may form a tentative classification for intermetallics based on the work herein, which may be given as:

Noble particles with high electrochemical activity, *e.g.*, Al$_2$Cu, Al$_7$Cu$_2$Fe. $E_{corr} > E_{corr}$ of alloy, with the ability to sustain large cathodic current. Such intermetallics are possibly associated to peripheral pitting.

Noble particles with low electrochemical activity, *e.g.*, Al$_3$Zr. $E_{corr} > E_{corr}$ of alloy, however, these particles do not sustain large cathodic currents and may be too small to adversely impact corrosion kinetics. Pitting is not often associated with these intermetallics.

Active particles with high self dissolution rates, *e.g.*, MgZn$_2$. $E_{corr} < E_{corr}$ of alloy, with the ability to undergo anodic dissolution at high rates.

Active particles with low self dissolution rates. Not observed here (although in a range of potentials, Mg$_2$Al$_3$ may qualify).

Active particles with a noble elemental component, *e.g.*, Al$_2$CuMg. Dealloying and incongruent dissolution may lead to polarity reversal. Can be selectively dissolved or lead to peripheral pitting.

The survey presented here may be utilized either independently or in conjunction with other localized measurement techniques to be applied to the problem of alloy corrosion. This work focuses on one specific aspect of localized corrosion in Al alloys, while in keeping with the presentation of a survey of results, a deliberate effort has been made not to discuss other factors such as local pH, transition from metastable to stable pits, pit chemistry, etc.

Conclusions

The information provided herein is a rich resource for clarification pertaining to the electrochemical behavior of Al alloys. It has been shown that the electrochemical microcell method was capable of distinguishing between the electrochemical behavior of intermetallics, pure elements, and solid solutions common to Al alloys.

Overall we can begin to develop a classification system for intermetallics based on more than relative activity or nobility that might be guessed from composition or measurement of corrosion potential. This classification is based on intermetallic passivity or activity, corrosion potential, corrosion current, and breakdown behavior.

Acknowledgments

References

1. I. J. Polmear, *Light Alloys*, 3rd ed., Arnold, London (1995).
2. R. G. Buchheit, *J. Electrochem. Soc.*, **142**, 3994 (1995).
3. F. Sato and R. C. Newman, *Corrosion (Houston)*, **55**, 3 (1999).
4. M. Zamin, *Corrosion (Houston)*, **37**, 627 (1981).
5. B. Mazurkiewicz and A. Piotrowski, *Corros. Sci.*, **23**, 697 (1983).
6. O. Seri, *Corros. Sci.*, **36**, 1789 (1994).
7. J. R. Scully, T. O. Knight, R. G. Buchheit, and D. E. Peebles, *Corros. Sci.*, **35**, 185 (1993).
8. K. Nişancioğlu, *J. Electrochem. Soc.*, **137**, 69 (1990).
9. M. J. Pryor and J. C. Fister, *J. Electrochem. Soc.*, **131**, 1230 (1984).
10. A. Afseth, J. H. Nordlien, G. M. Scamans, and K. Nişancioğlu, *Corros. Sci.*, **44**, 2543 (2002).
11. J. L. Searles, P. I. Gouma, and R. G. Buchheit, *Metall. Mater. Trans. A*, **32A**, 2859 (2001).
12. G. O. Ilevbare and J. R. Scully, *Corrosion (Houston)*, **57**, 134 (2001).
13. G. O. Ilevbare and J. R. Scully, *J. Electrochem. Soc.*, **148**, 196 (2001).
14. C. M. Liao, J. M. Olive, M. Gao, and R. P. Wei, *Corrosion (Houston)*, **54**, 451 (1998).
15. E. McCafferty, *J. Electrochem. Soc.*, **150**, 238 (2003).
16. M. Büchler, T. Watari, and W. H. Smyrl, *Corros. Sci.*, **42**, 1661 (2000).
17. G. O. Ilevbare, O. Schneider, R. G. Kelly, and J. R. Scully, *J. Electrochem. Soc.*, **151**, 453 (2004).
18. O. Schneider, G. O. Ilevbare, R. G. Kelly, and J. R. Scully, *J. Electrochem. Soc.*, **151**, 465 (2004).
19. T. J. R. Leclère and R. C. Newman, *J. Electrochem. Soc.*, **149**, 52 (2002).
20. R. G. Buchheit, L. P. Montes, M. A. Martinez, J. Michael, and P. F. Hlava, *J. Electrochem. Soc.*, **146**, 4424 (1999).
21. L. F. Mondolfo, *The Aluminum-Magnesium-Zinc Alloys*, Research and Development Center, Revere Copper and Brass Inc., Rome, NY (1967).
22. S. P. Ringer and K. Raviprasad, *Mater. Forum*, **24**, 59 (2000).
23. *Aluminum: Properties and Physical Metallurgy*, J. E. Hatch, Editor, ASM, Metals Park, OH (1984).
24. Q. Meng and G. S. Frankel, *J. Electrochem. Soc.*, **151**, 271 (2004).
25. J. A. Wert, *Scr. Metall.*, **15**, 445 (1981).
26. S. K. Maloney, K. Hono, I. J. Polmear, and S. P. Ringer, *Scr. Mater.*, **41**, 1031 (1999).
27. M. Gao, C. R. Feng, and R. P. Wei, *Metall. Mater. Trans. A*, **29A**, 1145 (1998).
28. Y. Yoon, PhD Thesis, The Ohio State University, Columbus, OH (2004).
29. N. Birbilis and R. G. Buchheit, Unpublished data.
30. R. G. Buchheit, M. A. Martinez, and L. P. Montes, *J. Electrochem. Soc.*, **147**, 119 (2000).
31. V. O. Lavrenko, V. A. Shvets, S. O. Firstov, S. B. Prima, V. O. Kochubei, and V. M. Adeev, *Powder Metall. Met. Ceram.*, **42**, 291 (2003).
32. R. G. Buchheit, R. K. Boger, M. C. Carroll, R. M. Leard, C. Paglia, and J. L. Searles, *JOM*, **53**, 29 (2001).
33. M. Paljević, *J. Less-Common Met.*, **175**, 289 (1991).
34. R. M. Leard, M.Sc. Thesis, The Ohio State University, Columbus, OH (2001).
35. R. G. Buchheit, R. P. Grant, P. F. Hlava, B. McKenzie, and G. L. Zender, *J. Electrochem. Soc.*, **144**, 2621 (1997).
36. C. M. Liao and R. P. Wei, *Electrochim. Acta*, **45**, 881 (1999).
37. P. Leblanc and G. S. Frankel, *J. Electrochem. Soc.*, **149**, 239 (2002).
38. F. Andreatta, H. Terryn, and J. H. W. de Wit, *Corros. Sci.*, **45**, 1773 (2003).
39. F. Andreatta, H. Terryn, and J. H. W. de Wit, *Electrochim. Acta*, In press (2004).
40. S.-M. Moon, S. Sakairi, and H. Takahashi, *J. Electrochem. Soc.*, **151**, 399 (2004).
41. J. C. Seegmiller and D. A. Buttry, *J. Electrochem. Soc.*, **150**, 413 (2003).
42. F. Andreatta, M. M. Lohrengal, H. Terryn, and J. H. W. de Wit, *Electrochim. Acta*, **48**, 3239 (2003).
43. T. Suter and H. Böhni, *Electrochim. Acta*, **43**, 2843 (1998).
44. T. Suter and H. Böhni, *Electrochim. Acta*, **47**, 191 (2001).
45. M. M. Lohrengal, *Corrosion Engineering Science and Technology*, **39**, 53 (2004).
46. T. Suter and R. C. Alkire, *J. Electrochem. Soc.*, **148**, 36 (2001).
47. E. McCafferty, *Corros. Sci.*, **37**, 481 (1995).
48. *Corrosion of Aluminum and Aluminum Alloys*, J. R. Davis, Editor ASM, Materials Park, OH (1999).
49. Z. Szklarska-Smialowska, *Corros. Sci.*, **41**, 1743 (1999).